Large-scale graph networks and AI applied to medical image data processing

Meyer-Bäse, Anke, Foo, Simon, Tahmassebi, Amirhessam, Meyer-Bäse, Uwe, Moradi Amani, Ali, et al.

Anke Meyer-Bäse, Simon Foo, Amirhessam Tahmassebi, Uwe Meyer-Bäse, Ali Moradi Amani, Theresa Götz, Doris Leithner, Andreas Stadlbauer, Katja Pinker, "Large-scale graph networks and AI applied to medical image data processing," Proc. SPIE 11396, Computational Imaging V, 1139605 (21 May 2020); doi: 10.1117/12.2557813

Event: SPIE Defense + Commercial Sensing, 2020, Online Only, California, United States

Large-Scale Graph Networks and AI Applied to Medical Image Data Processing

Anke Meyer-Bäse[a], Simon Foo[b], Amirhessam Tahmassebi[a], Uwe Meyer-Bäse[b], Ali Moradi Amani[c], Theresa Götz[d], Doris Leithner[e], Andreas Stadlbauer[f] and Katja Pinker-Domenig[a,g,h]

[a] Department of Scientific Computing,
Florida State University, Tallahassee, Florida 32310-4120, USA
[b] Department of Electrical and Computer Engineering,
Florida A&M University and Florida State University, Tallahassee, Florida 32310-4120, USA
[c] School of Engineering, RMIT University, Melbourne, Victoria 3001, Australia
[d] Pattern Recognition Laboratory, University Erlangen-Nürnberg, 91054 Erlangen, Germany
[e] University Hospital Frankfurt, Institute for Diagnostic and Interventional Radiology 60590 Frankfurt am Main, Germany
[f] Department of Neurosurgery, University Erlangen-Nürnberg, 91054 Erlangen, Germany
[g]Department of Biomedical Imaging and Image-guided Therapy, Molecular and Gender Imaging, Medical University of Vienna, Vienna, Austria
[h] Department of Radiology, Breast Imaging Service, Memorial Sloan-Kettering Cancer Center, New York, USA

ABSTRACT

With the increasing amount of available medical data, computing power and network speed, modern medical imaging is facing an unprecedented amount of data to analyze and interpret. Phenomena such as Big Data-omics stemming from several diagnostic procedures and novel multi-parametric imaging modalities tend to produce almost unmanageable quantities of data. The paper addresses the aforementioned context by assuming that a novel paradigm in massive data processing and automation becomes necessary in order to improve diagnostics and facilitate personalized and precision medicine for each patient. Traditional machine learning concepts have demonstrated many shortcomings when it comes to correctly diagnose fatal diseases. At the same time static graph networks are unable to capture the fluctuations in brain processing and monitor disease evolution. Therefore, artificial intelligence and deep learning are increasingly applied in oncologic medical imaging because they excel at providing quantitative assessments of biomedical imaging characteristics. On the other hand, novel concepts borrowed from modern control have paved the path for a dynamic graph theory that can predict neurodegenerative disease evolution and replace longitudinal studies. We chose two important topics, brain data processing and oncologic imaging to show the relevance of these concepts. We believe that these novel paradigms will impact multiple facets of radiology but are convinced that it is unlikely that they will replace radiologists any time in the near future since there are still many challenges in the clinical implementation.

Keywords: Dynamic graph theory, radiomics, convolutional neural network, artificial intelligence, imaging connectomics, neurodegenrative disease, cancer

1. INTRODUCTION

The last decade in medical imaging has been shaped by the "Big Data" era and has seen an enormous growth in applications of large-scale graph networks in brain research, and artificial intelligence (AI) and deep learning (DL) in radiology. This contribution aims to elucidate the existing challenges in the two above-mentioned fields - brain research and oncologic imaging - and to unveil novel methods from graph networks and AI and DL applicable to these emerging fields.

Brain research has seen an increase in the available relational data recorded from couplings and interactions among the elements of the neural system. Most of the studies are descriptive and focus on pairwise interactions

Computational Imaging V, edited by Lei Tian, Jonathan C. Petruccelli, Chrysanthe Preza, Proc. of SPIE Vol. 11396, 1139605 · © 2020 SPIE
CCC code: 0277-786X/20/$21 · doi: 10.1117/12.2557813

captured by static graphs with dyadic links. Pearson correlation is the basis of establishing links between the nodes of the graph. However to capture the dynamic integration arising from considering at the same time the structural topology of the brain networks and the dynamics of functional connectivity, novel processing paradigms become necessary that include the changes in the topology and connections over time. An important example are the cortical hub regions that describe the "dynamic core network" comprising hubs changing over time their centrality between high and low.

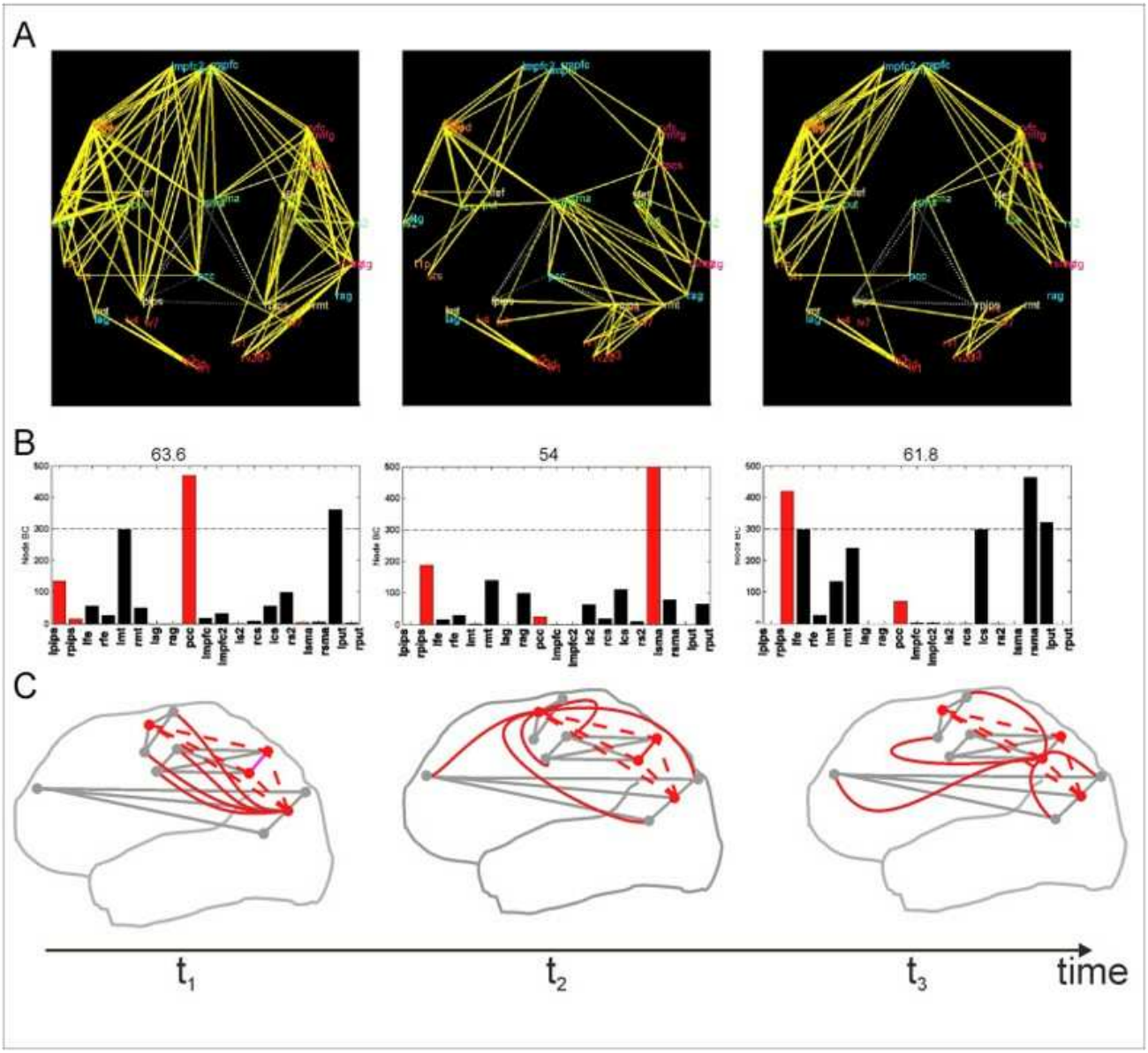

Figure 1. The dynamic core network showing the change of functional hubs over time. Reprinted with permission from.[15]

The challenges in medical imaging and computational radiology include the simultaneous evaluation of imaging, molecular and liquid biopsy data from a patient, the evaluation of radiation and chemotherapy from multimodal imaging techniques as well as the quick diagnosis and detection from hybrid imaging. To respond to these challenges different strategies have been applied: artificial intelligence, radiomics or a combination of both. Radiomics means a conversion of images from different imaging techniques into mineabale data. There are several benefits associated with quantitative radiomics: (1) establishing predictive image-based phenotypes of a

disease for translational and precision medicine and (2) creating quantitative image-based phenotypes for data mining with other existing omics for data discovery. A well-known example is imaging genomics. The difference between AI and radiomics is shown in Figure 2: AI works directly with images while radiomics employs computer-extraction of "handcrafted" features. In addition fast architectures have been developed to tackle the high-speed data evaluation.[57, 59, 60, 62, 63]

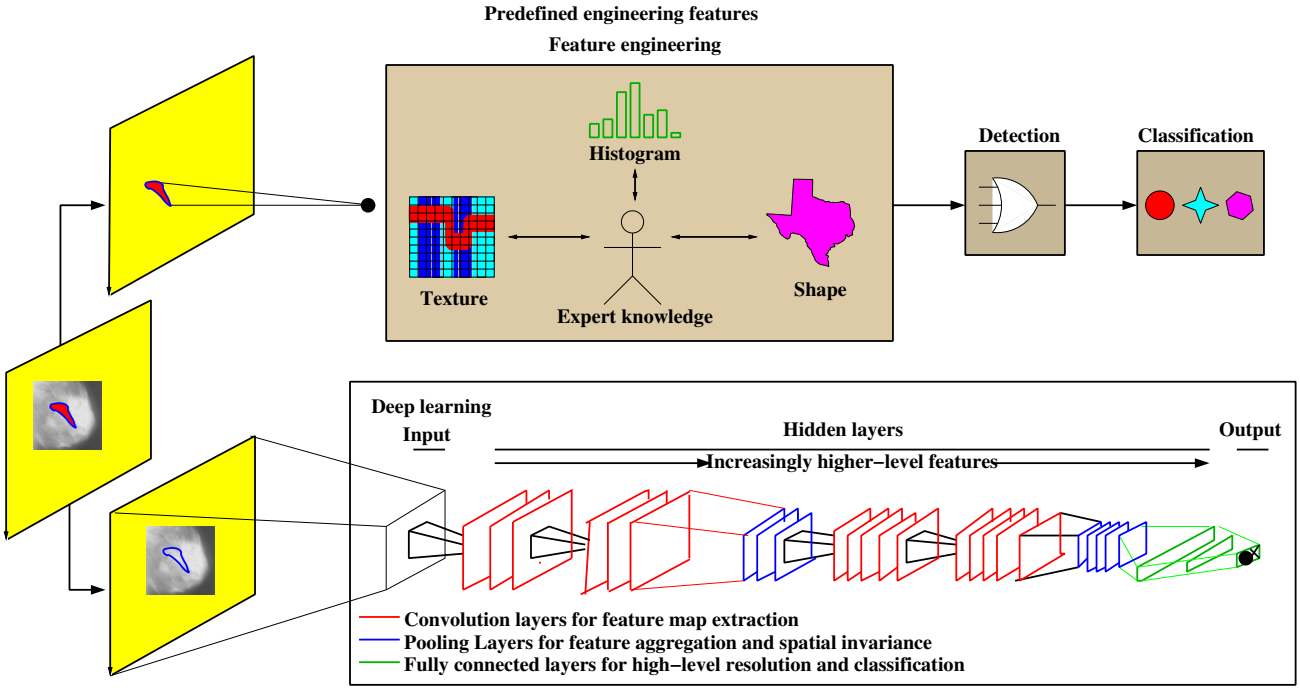

Figure 2. Differences between conventional and deep learning in mammography for the lesion discrimination task. The upper part of the image represents the traditional radiomics-based processing. Features such as texture, shape and histogram are fused to describe the tumor. These features require expert knowledge and are so-called engineered features. The lower part shows the DL-based processing and does not require any annotation. The whole image is analyzed and through several deeper layers information from low level (edges) to high level (objects) is obtained.

2. APPROACH

2.1 Novel Dynamic Graph Networks Paradigms

New control paradigms become imperative when analyzing and interpreting vast experimental data sets and explain synchronization phenomena in human brain networks. Graph theory represents a powerful method to visualize[49] and target in combination with modern control theory relevant nodes in the resulting graph. We pioneered the application of modern control paradigms as a method to capture the temporal dynamic changes in brain networks.[48, 52]

Mathematically, graph networks are defined as relations among a bounded set of nodes with the typical data model being a graph $G = (V, E)$ with vertices V and edges E representing relations between the nodes. In addition to graph theory, the empirical nature of the field imposes statistical approaches as a complementary tool. While static graphs give a snapshot of a single representation, dynamic graphs describe the temporal evolution of relations among nodes as shown in Figure 3.

2.1.1 Pinning Control in Imaging Connectomics

Network controllability is becoming an important area in functional networks. The current methods applicable to analyze these networks are nonlinear dynamical graph theory to determine driver nodes in networks or reach a consensus.[4, 5, 42, 88]

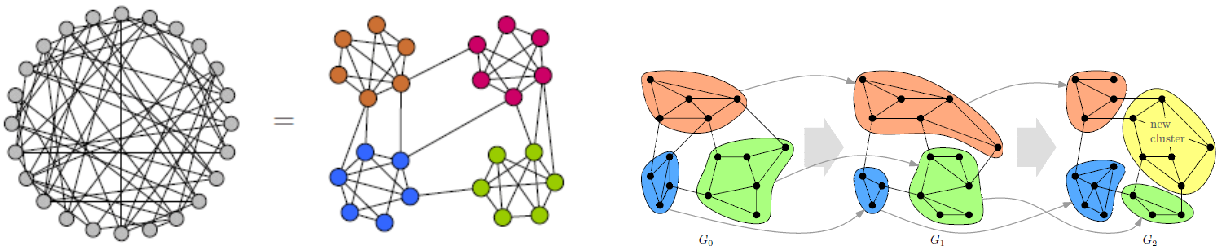

(a) (b)

Figure 3. Graph structures. (a) Graphs excel at hiding their structure. Graph clustering aims at revealing their structure. (b) Time-dependent graph clustering. Three time steps of a dynamic graph: smooth dynamic clustering and cluster tracking over time (gray arrows).[23]

The most intriguing question when analyzing a dynamic graph network is the role of each node. To reach therapeutic efficacy we need to "drive" a regulatory network from an existing disease-state to an optimal disease-free state. The complexity of the networks poses many limitations to traditional analysis tools:[46] (1) most graph networks are directed, (2) the size of the network does not allow testing of several combinations to determine driver nodes, and (3) the weights between nodes are not equal and time-dependent. Modern control theory[42,88] provides many tools to control such a network and thus successfully implement a therapeutic strategy. In the parlance of control theory, tools are described that are able to identify the set of driver nodes and thus guide the network's entire dynamics.

We introduce a weighted directed graph $G = (V, E, A)$ of order N that has a set of nodes $V = \{v_1, \cdots, v_N\}$, a set of directed edges $E \subseteq V \times V$, and a weighted adjacent matrix $A = (a_{ij})_{N\times N}$ where a_{ij} represent the weight of link from node i to j. The Laplacian matrix $L = (L_{ij})_{N\times N}$ of the graph is defined as $L_{ij} = -a_{ij}$ for $i \neq j$, with $i, j \in \{1, \cdots, N\}$ and $L_{ii} = k_i^{out}$ for $i \in \{1, \cdots, N\}$, and $k_i^{out} = \sum_{j=1, i\neq j}^{N} a_{ij}$, represents the sum of all afferent edges. It's evident that $\sum_{j=1}^{N} L_{ij} = 0$ for all $i = 1, 2, \cdots, N$.

We define the consensus problem as a modality to reach an agreement between a group of autonomous agents, in our case the nodes, when these change dynamically.

Mathematically, the consensus protocol in a multi-node system is defined as:

$$\dot{x_i}(t) = \sum_{j\neq i} a_{ij}(x_j(t) - x_i(t)) = -\sum_{j=1}^{N} L_{ij}x_j(t) \tag{1}$$

where $x_i(t) \in R^n$ is the state of the node. $L = L(t)$ is a time-varying matrix when the graph network topology changes over time.

Assuming that the dynamics of the node is nonlinear,[83] then the state equation becomes

$$\dot{x_i}(t) = f(x_i(t)) - c\sum_{j=1}^{N} L_{ij}\Gamma x_j(t) \tag{2}$$

with $f() \in R^n$ representing the nonlinearity, c the coupling strength, and $\Gamma = diag(\gamma_1, \cdots, \gamma_n) \in R^{n\times n}$ being a semi-positive definite diagonal matrix with $\gamma_j \geq 0$. If $\gamma_j \neq 0$ means that the nodes can communicate through their jth state.

A desired trajectory to be reached by the system, corresponding to a therapeutical solution, is defined as

$$\dot{s}(t) = f(s(t)) \tag{3}$$

where $s(t)$ is an isolated equilibrium point. To achieve this equilibrium point, the new evolving equation becomes

$$\dot{y_i}(t) = f(x_i(t)) - f(s(t)) - c\sum_{j=1}^{N} L_{ij}\Gamma y_j(t) \tag{4}$$

where $y_i = x_i - s_i$. The pinning control strategy is to guide the network to the desired state $s(t)$. The controllability of the system is evaluated based on the algebraic connectivity. Measures derived from the smallest and largest eigenvalue of the connecting matrix are essential to determine the success of controllability. The number of controlling nodes is smaller than the number of total nodes in the network and a direct control is possible only at these nodes and then propagated to the rest of network through vertices.

The theoretical results in[42,88] have shown that: (a) nodes with low degrees should be pinned first and not hubs, which are usually of high degree, and (b) the minimum number of nodes to be selected for control can be theoretically determined. In large real-world networks, however, the detection of controlling regions becomes a constrained optimization problem.[82] These results are valid for both directed and undirected graphs.

2.1.2 Model Reduction of Brain Connectivity Networks

Novel mathematical concepts such as graph theoretical techniques can capture the brain connectivity and its topology.[19,21,89] These graph networks are mostly based on Pearson correlation and are capturing either the structural and/or functional brain connectivity. From these graphs, new descriptors can be derived to quantify induced changes in topology or network organization, or serve as theory-driven biomarkers to predict dementia at the level of the individual subject.

Most graph networks applied to dementia research, even for longitudinal data, are static graph networks which cannot capture the dynamical processes governing the time evolution of neurodegenerative diseases. Therefore, a new paradigm in neurodegenerative diseases research - dynamical graph networks - is required to advance this field and overcome the obstacles posed by static graph theory in terms of disease prediction, evolution, and its associated connectivity changes.

To address this important issue of analyzing the dynamical behavior, we propose a simplified method resulting in a model of lower complexity. Balanced truncation is known as the standard method for model reduction.[64] It is based on a state–space point of view of employing the well–known observability and controllability Gramians[35,61,73] and related to the past input energy (controllability) and future input energy (observability). While for linear systems this procedure is pretty straightforward, for nonlinear systems balancing truncation becomes in general not a simple task.[55,58] However they are not quite efficient in terms of model reduction for large-scale networks. For brain connectivity models, we require a structure preservation between subsystems and at the same time, a network topology-preserving mechanism to provide model reduction. We will address this issue by choosing a technique based on an area aggregation and time-scale modeling for sparse brain networks with densely interconnected hubs and externally sparse interconnections between these hubs. In[12] it was shown that the neurons in the hubs synchronize on the fast time-scale and as aggregated neurons determine the slow dynamics of the neural network. The idea of two-time scale systems has been widely studied in connections with dynamical systems.[48,51,53,54,56,70]

Graph networks can exhibit a structure of dense clustered areas but have sparse connections between these areas as shown in Figure 3a. They can be dynamically approximated by a two-time scale system, where the neurons within the same area synchronize on the fast time-scale, because the dense within-area connections drive the nodes of the given area quickly to reach an equilibrium.

At the same time, the exchange between the areas is based on sparse connections and can be described at a slow time-scale. This coupled dynamics leads to a reduced-order model describing the long-term behavior of the overall network. The large-scale brain network is viewed as an interconnected graph with links between the areas which are viewed as nodes in the graph.

2.2 AI-Based Methods Used in Radiology

2.2.1 Data-Driven Approaches

Data-driven approaches are based on collecting medical imaging or signal data and extracting meaningful features for the subsequent classification. Most approaches in imaging connectomics and oncologic imaging do not utilize a-priori information for the classification task. These techniques are classified into two categories: supervised and unsupervised.

For supervised learning, not only the input data but also the corresponding target answers are presented to the classifier. Learning is done by the direct comparison of the actual output of the classifier with known correct answers. This is also referred to as learning with a teacher. In contrast, if only input data without the corresponding target answers are presented to the classifier for learning, we have unsupervised learning. In fact, the learning goal is not defined at all in terms of specific correct examples. The available information is in the correlations of the input data. The network is expected to create categories from these correlations and to produce output signals corresponding to the input category. Table 1 gives an overview of data-driven techniques used in imaging connectomics and cancer radiology.

Table 1. Brief overview of common data-driven techniques used in imaging connectomics and cancer radiology.

Technique	Advantages	Disadvantages	References
Supervised learning			
Ensemble of decision trees	Decision using branches Variable significance and feature selection are included	Useful for prediction Problem is overfitting	10, 39, 80 2
Random forest	Improved performance compared to decision trees	Increase in bias	3, 67, 80
Naive Bayesian	Easy to understand Fast	Numeric attributes follow normal distribution Less accurate	16, 25 31, 74 14, 24
Support vector machines	Transforms non-linear classification problem into linear one. High accuracy.	Binary classifier. Difficult computation in high-dimensional data space.	27, 66 6, 20, 34
Neural networks	Weights need to be adapted for training. Multi-class classification.	No strategy to determine network structure.	18, 45, 79 11, 28 29, 69
Deep learning	State-of-the art in image-derived features.	Computationally intensive. Hard to interpret.	7, 68 13, 40, 91 8, 30, 90
Unsupervised learning			
Clustering (k-means)	Brief training duration.	Number of clusters must be known in advance.	75, 78
Topological data analysis	Interpretable data mapping. Discovery of variables relationships.	Divided clusters due to mapping.	11, 43, 47

2.2.2 Radiomics-Based Approaches

In the past two years, a novel computational approach - radiomics - emerged to represent oncological tissues based on quantitative descriptors.[1] It has been hypothesized that a large number of radiomic features tremen-

dously increase prognostic power. With the increasing importance of "personalized medicine", new treatment strategies are being sought to respond to the specific characteristics of each patient and cancer phenotype. So far personalized medicine is centered around molecular characteristics with genomics and proteomics data analysis.

Radiomics represents a novel approach to achieve a detailed quantification of the tumor phenotypes by analyzing a large number of image descriptors. In Hoffman et al.,[26] a quantitative radiomics approach was applied based on shape, texture and MRI tumor features and evaluated in comparison with a reduced-order feature approach in a CAD system applied to diagnostically challenging breast lesions.

The potential of radiomics as a training-independent diagnostic decision tool was shown in Bickelhaupt et al.[9] The radiomics classifiers performed well in the differentiation of malignant and benign lesion, however their performance was lower than that of an experienced radiologist. Prasanna et al.[67] introduced a new radiomics descriptor, the Co-occurrence of Local Anisotropic Gradient Orientations (CoLlAGe). It is able to distinguish benign and pathologic phenotypes when they appear similar to each other on anatomic imaging. This new descriptor can capture their local entropy patterns and thus reflect hidden local differences in tissue microarchitecture.

Another study[71] analyzed the effect of varying MRI scanner parameters on breast lesions and found that fibroglandular tissue in feature extraction radiomics studies is more susceptible to imaging parameters than breast tumors.

2.2.3 Deep Learning and Convolutional Neural Networks

Deep learning belongs to the so-called class of representation learning in machine learning and is based on modeling high-level abstractions in data by using many more hidden layers than the standard "shallow" neural networks. These layers have complex structures and employ multiple non-linear transformations. The most important fact about DL is that they replace the "engineered" features of traditional machine learning with hierarchical feature extraction. The best known architecture in DL is the convolutional neural network (CNN).[38,72] Learning can be both supervised or unsupervised. Higher level features are derived from lower level features in form of a hierarchical processing. A typical DL network architecture is shown in Figure 4.

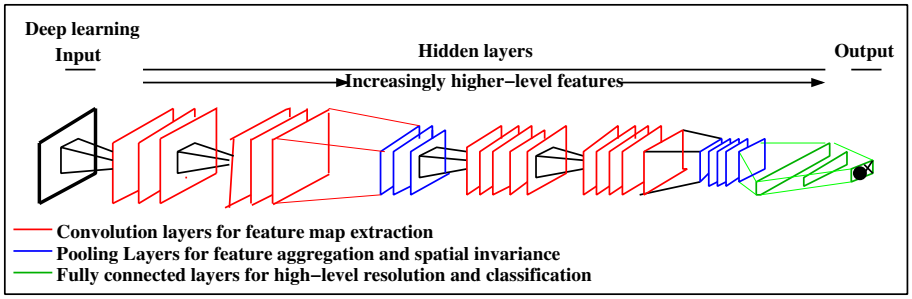

Figure 4. Deep learning network. The information flow goes from the first layer to the last layer similarly to the traditional neural networks. However, the layers have an increasing level of abstraction. The classification result is a unique shape that can be assigned to the object to be recognized.

3. RESULTS

3.1 Dynamical Graph Theory Networks Techniques for the Analysis of Sparse Connectivity Networks of Cortical Thickness

Structural and functional networks give us an important insight into brain development and organization. The standard measure of pairwise correlations are Pearson product-moment correlation coefficients $P = (\rho_{ij})$, which quantify the linear dependency between two variables l_i and l_j. Pearson correlation networks have been widely applied in imaging connectomics,[19,85] bioinformatics[17,50,53] and in addiction research.[41,77,81,87] A common problem of Pearson correlation coefficients are indirect effects giving rise to a plethora of unspecifically high correlation coefficients. Partial correlation networks attempt to estimate conditional dependencies between measured variables over all samples rather than marginal dependencies, thereby eliminating such indirect correlations.

Translated to brain networks, interacting pairs of regions in this nertwork can be better detected by partial correlations than by the standard methods. A robust algorithm for partial correlations, the so-called PC* proposed in,[84] is a graph pruning algorithm for identification of these correlations avoiding the direct calculation of partial correlations from the inverse of the sample correlation matrix.

We apply dynamical graph theory on structural concentration and PC* connectivity graphs from[84] for the lateral views of the left and right hemispheres. For the connectivity networks, the cortical gray matter thickness derived from 645 automatically parceled cortical volumes from $T1$-images is analyzed. 25 parceled regions are analyzed per hemisphere.

Cortical gray matter thickness is an important morphological feature when it comes to the study of brain connectivity. Many relevant brain phenomena such as aging, schizophrenia, and Alzheimer's consider cortical thickness correlations.

The covariation in cortical thickness in ROIs defined on a parceled cortex is represented in such graphs either as a simple concentration or as a PC*. The nodes in the graphs represent the ROIs while the links show if a connection is existing between these regions or not.

Figure 5 shows the clusters found on the functional data for the lateral view of the left and right hemispheres. We perform a time-scale modeling and area aggregation with two main areas on the four functional networks from Figure 5. For three graphs we can apply Theorem 1, however for the concentration graph, lateral view of left hemisphere, we are not able to obtain an area aggregation since the conditions in Theorem 1 are not satisfied.

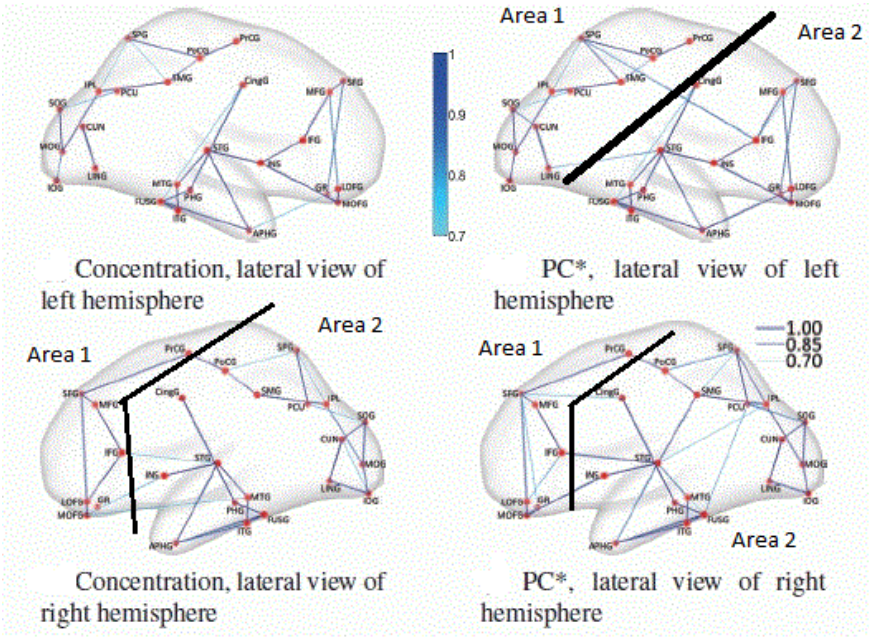

Figure 5. Areas of the connectivity graph for the concentration and PC* graphs for the left and right hemispheres comprising 25 parcellated cortical regions from the left and right hemispheres and number of theoretically determined driver nodes N. Figure adapted from.[84]

The results of the in-depth dynamical analysis are shown in Table 2. The PC* show smaller node and area parameters than the concentration graphs. But most importantly, both the exact, as well as the rigid aggregate model show the same eigenvalues for both graphs of the right hemispheres.

While the results obtained through PC* show a better aggregated structure than the concentration graph in terms of node and area parameter, the dynamic graph analysis reveals no different slow modes between concentration and PC*. The eigenvalues in the right hemisphere are larger than those in the left hemisphere. The contribution of the larger eigenvalues over time decreases quickly. The range of the eigenvalues for each

Correlation	Node Parameter d	Area Parameter δ	Slow λ exact system	Slow λ rigid aggregate system
Pearson Corr. left	$d_{ave} = 0$	$\delta = 0$	N/A	N/A
PC left	$d_{ave} = \frac{1}{6}$	$\delta = \frac{1}{12}$	$\lambda_i = \{0, -4\}$	$\lambda_i = \{0, -25/77\}$
Pearson Corr. right	$d_{ave} = \frac{4}{7}$	$\delta = \frac{2}{7}$	$\lambda_i = \{0, -8\}$	$\lambda_i = \{0, -50/63\}$
PC right	$d_{ave} = \frac{1}{2}$	$\delta = \frac{1}{4}$	$\lambda_i = \{0, -8\}$	$\lambda_i = \{0, -50/63\}$

Table 2. Area aggregation parameters and time-scale modeling for correlation graphs from Figure 5. The graphs are for the left and right hemisphere.

subject represents an important biomarker for disease prediction. By providing an area and node parameter, we are able to add additional static graph descriptors to the dynamic biomarkers.

3.2 Radiomics-Based Computer-Aided Diagnosis of Diagnostically Challenging Lesions in Breast MRI

Diagnostically challenging lesions pose a difficulty for both for the radiological reading and for current CAD systems. They are poorly defined in both morphology (geometric shape) and kinetics (temporal enhancement) and pose a challenge to lesion detection and classification. Their strong phenotypic differences can be visualized by MRI. Figure 6 shows in 3D the differences in both spatial and temporal behavior between these lesions.

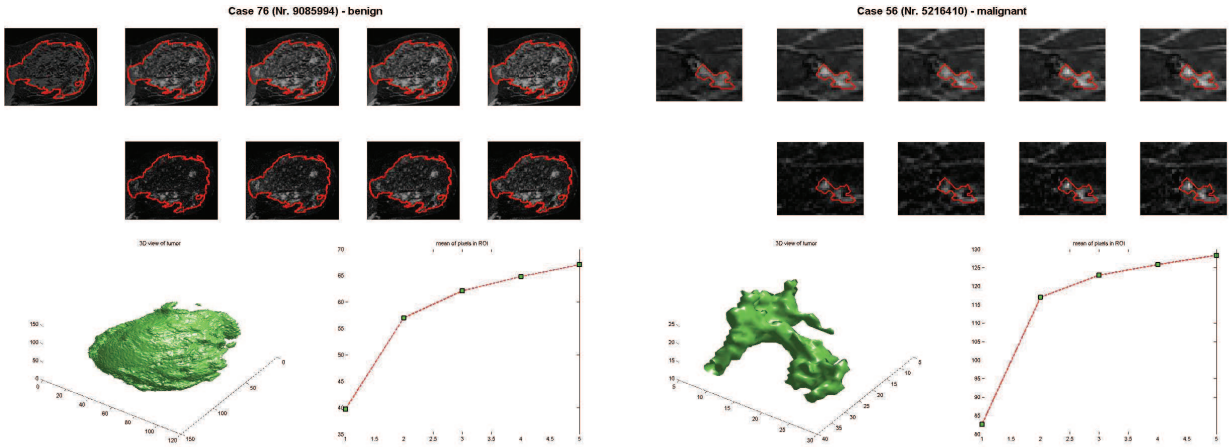

(a) Benign (b) Malignant

Figure 6. Morphological and dynamic representations of segmented benign (diffusely enhancing glandular tissue) and malignant (invasive ductal carcinoma) non-mass-like-enhancing lesions. The time-scans in the first row are without motion compensation while those in the second row are motion-corrected.

Radiomics represents a novel approach to achieve a detailed quantification of the tumour phenotypes by analyzing a large number of image descriptors. A computer-aided diagnosis system can determine quantitatively the utility of the radiomics approach to diagnostically challenging lesions in breast MRI compared to the standard reduced-order feature approach.

We extract both kinetic and morphological features to better capture the heterogeneity of the diagnostically challenging lesions. Diagnostically challenging lesions have kinetic characteristics that are far less well characterized and of limited accuracy in discriminating between malignant and benign behavior.[33] As a dynamical feature, the slope of the relative signal intensity enhancement (RSIE) is used in most current CAD systems. Besides the description of the texture we also want to characterize the enhancement of the tumor due to the contrast agent. We are focussing on this in the following mainly by considering the mean gray-values of each tumor region and how it develops over time. Therefore we consider trivial facts like the magnitude of the enhancement as well as

more sophisticated methods like the Fourier transform or regression methods. The kinetic features considered for lesion description are found in the Table (3) under (b), (c), (g), (k), (l), (m) and (n).

Morphological characteristics contain valuable information about a lesion's type. Combined with kinetic properties, one could expect a higher accuracy. Furthermore, non-mass enhancing lesions such as DCIS or ILC can be better differentiated based on morphological properties.[65] We mostly consider features that describe the geometric local characteristics of the shape to identify the non-smooth surface. Therefore, we will focus on features that are solely based on the morphology of the tumor, i.e. we will study the geometric structure without considering the gray-values. The morphological features considered for lesion description are found in the Table (3) under (a), (d), (e), (f), (h), (i), (j), (o) and (p).

An overview of the morphological and kinetic features and their respective dimensionality is found in Table 3.

Label	**Feature types**	**Dimension**
(a)	Laplacian and eigenvalues of structure tensor	25
(b)	Regression with function as proposed in[33]	7
(c)	First order statistics	25
(d)	Fourier transformation of relative enhancement	5
(e)	Gabor features	300
(f)	Krawtchouk moments[86]	256
(g)	Regression with function as proposed in[22,44]	4
(h)	Geometric moments	9
(i)	Morphology	9
(j)	Scaling index[32]	25
(k)	Second order statistics	60
(l)	Slope of mean values	4
(m)	Regression with linear function	1
(n)	Fourier transformation	25
(o)	Writhe number[36,37]	5
(p)	Averaged Zernike descriptors over time[76]	122
		Total: 882

Table 3. Overview over all features.

We analyze quantitatively the effect of the large number of radiomic features on the detection and classification accuracy and compare it with a reduced-order feature vector describing best morphological or the temporal characteristics of diagnostically challenging lesions. We use either the total of 882 features or distinctive features to extract parameters from the temporal enhancement as well as parameters from the shape. We choose as a classifier a SVM with different kernels as described in Table 4. The area under the ROC curve (AUC) will serve as a quantitative evaluation measure for the CAD system employed for comparisons purposes.

SVM Kernel 1	SVM Classification with a Linear Kernel.
SVM Kernel 2	SVM Classification with a Polynomial Kernel.
SVM Kernel 3	SVM Classification with Radial Basis Kernel.
SVM Kernel 4	SVM Classification with Sigmoidal Kernel.

Table 4. Classifiers employed for lesion classification.

Figure 7 shows the classification results for all 822 features describing both morphology and kinetics of the lesions. The radiomic feature vector achieves a maximal AUC=0.55.

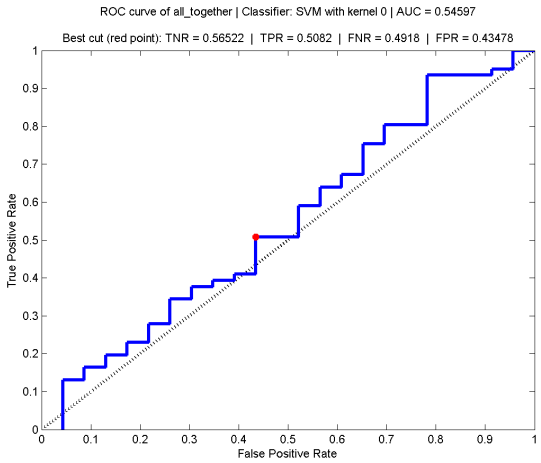

Kernel 1 (AUC= 0.55).

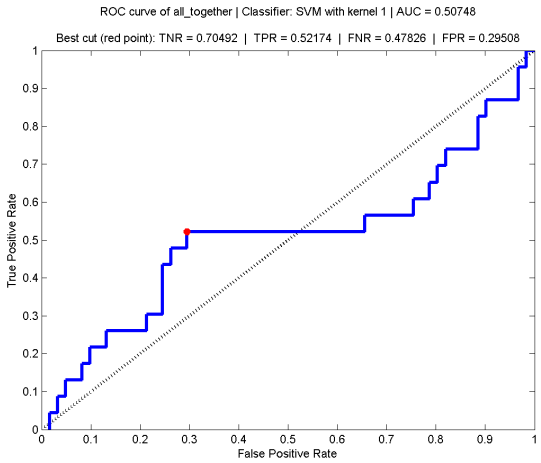

Kernel 2 (AUC= 0.51).

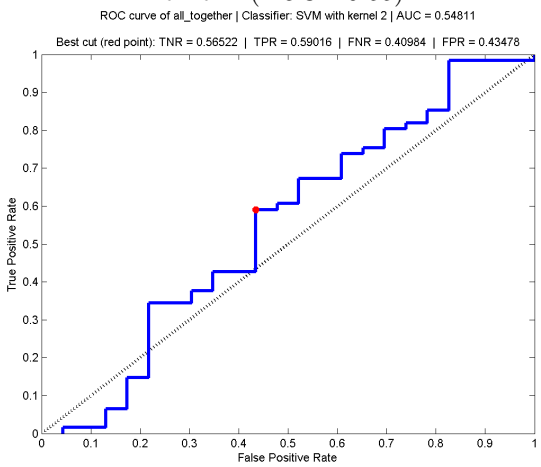

Kernel 3 (AUC= 0.55).

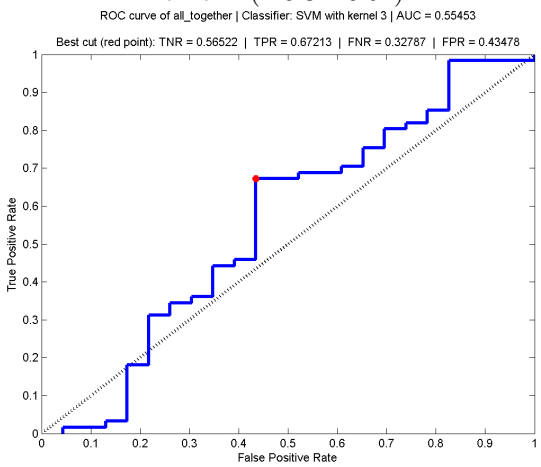

Kernel 4 (AUC= 0.55).

Figure 7. ROC curves resulting from classification with SVM using all features together.

Figure 8 provides an overview of the classification results for both motion-compensated data (blue bars) as well as uncompensated data (red bars) for parameters extracted from the temporal enhancement (kinetics) and from the shape (morphology). The maximal AUC achieved by the reduced-order feature vector representing the temporal enhancement is of AUC=0.77 and thus significantly higher than the radiomic vector.

The results show that the achieved lower AUC value is attributed to the redundancy that is introduced by the fusion of all possible features in the radiomic signature. The temporal enhancement features are the key descriptors for detection and classification in an automated system.

4. DISCUSSIONS

Graph theory and DL have received great attention in the medical imaging field. Graph networks have proven to be crucial for understanding the architecture, development and evolution of brain networks. Emerging architectural designs like multilayer networks combine multi-omic data such as large-scale brain connectivity with gene expressions. Novel theoretical concepts introduced by the dynamic graph theory such as switching topologies can track fast changes in graph topology and organization of functional networks. AI and DL enable the discovery of morphological and or textural features in images solely from data. This paper presented the methodological aspects of modern graph theory methods and of AI and DL, and their applications in brain and cancer research.

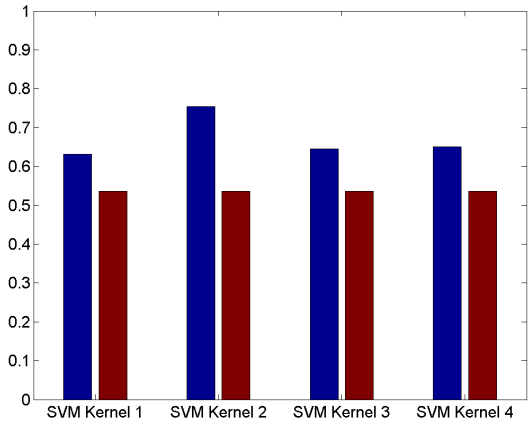

(a) Temporal enhancement descriptors

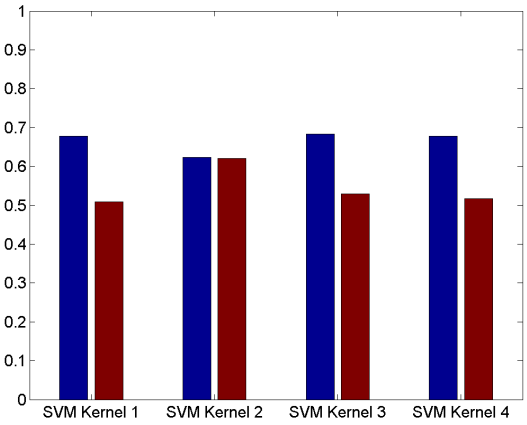

(b) Shape descriptors

Figure 8. AUCs of SVM applied to both temporal enhancement features and shape, separately, using four different kernels and both motion compensated (blue bars) as well as original data (red bars) to compute the features.

We showed the application of pinning control and reduced model of networked agents in simplifying the dynamics of brain networks and determining the critical "driver nodes" that may play an important role in disease evolution. Radiomics was applied to the computer-aided diagnosis of diagnostically challenging lesions and offered a full set of descriptive features for both morphological and temporal behavior of these lesions.

To summarize, modern dynamic graph theory and AI and DL may present many desirable advantages and strategies to solve challenges inherent to the big data-avalanche in medical imaging, and the increased demand stemming personalized and precision medicine. DL scales with the data, the more data are available, the more generalized features are obtained that can dramatically improve the performance of the automated detection or diagnosis system. The novel AI-driven architectures support associations like the human brain: the underlying methodological paradigm involves domain-specific knowledge. This exciting big data-driven research direction has still to overcome big challenges: (1) the plethora of novel and sophisticated graph models such as generative models, dynamic networks and multilayer networks need to be applied not only in basic but also in clinical and translational research, and (2) in DL the black box-like characteristics need to be abandoned such that an intuitive interpretation and understanding of the models becomes possible. We believe that these novel tools will help clinicians to provide better patient care.

5. ACKNOWLEDGMENTS

This paper is funded in part by an ONR grant N00014-18-1-2342.

REFERENCES

[1] H. Aerts, E. Velazquez, R. Leijenaar, C. Parmar, P. Grossmann, S. Carvalho, J. Bussink, R. Monshouwer, B. Haibe-Kains, D. Rietveld, F. Hoebers, M. Rietbergen, C. Leemans, A. Dekker, J. Quacjenbush, R. Gillies, and P. Lambin. Decoding tumour phenotype by noninvasive imaging using a quantitative radiomics approach. *Nature Communications*, 5:4644, 2 2014.

[2] S. Agliozzo, M. De Luca, C. Bracco, A. Vignati, V. Giannini, L. Martincich, A. Bert, F. Sardanelli, and D. Regge. Computer-aided diagnois for contrast-enhanced breast mri of mass-like lesions using a multiparametric model combining a selection of morphological, kinetic and spatio-temporal features. *Medical Physics*, 39:3102–3109, 4 2012.

[3] S. C. Agner, S. Soman, E. Libfeld, M. McDonald, K. Thomas, S. Englander, M. A. Rosen, D. Chin, J. nosher, and A. Madabhushi. Textural kinetics: A novel dynamic contrast-enhanced (dce)-mri feature for breast lesion classification. *Journal of Digital Imaging*, 24:446–463, 7 2011.

[4] A. Moradi Amani, M. Jalili, X. Yu, and L. Stone. Finding the most influential nodes in pinning controllability of complex networks. *IEEE Transactions on Circuits and Systems II*, 64:685–689, 8 2017.

[5] A. Moradi Amani, M. Jalili, X. Yu, and L. Stone. Controllability of complex networks: Choosing the best driver set. *Physical Review E*, 98:030302, 8 2018.

[6] D. Ampeliotis, A. Anonakoudi, K. Berberidis, and E. Psarakias. Computer aided detection of prostate cancer using fused information from dynamic contrast enhanced and morphlogical mangetic resonance imaging. *IEEE International Conference on Signal processing and Communication*, 2:888–891, 7 2007.

[7] N. Antropova, H. Abe, and M. Giger. Use of clinical mri maximum intensity projections for improved breast lesion classification with deep convolutional neural networks. *Journal of Medical Imaging*, 5:014503, 2018.

[8] N. Antropova, B. Huynh, and M. Giger. Recurrent neural networks for breast lesion classification based on dce-mris. *SPIE Medical Imaging*, 10575:UNSP10575M, 2018.

[9] S. Bickelhaupt, D. Paech, P. Kickingereder, F. Steudle, W. Lederer, H. Daniel, M. Gotz, N. Gahlert, D. Tichy, M. Wiesenfarth, F. B. Laun, K. Maier-Hein, H. Schlemmer, and D. Bonekamp. Prediction of malignancy by a radiomic signature from contrast agent-free diffusion mri in suspicious breast lesions found on screening mammography. *Journal of magnetic resonance imaging*, 46(2):604–616, 2017.

[10] N. Braman, M. Etesami, P. Prasanna, C. Dubchuk, H. Gilmore, P. Tiwari, D. Plecha, and A. Madabushi. Intratumoral and peritumoral radiomics for the pretreatment prediction of pathological complete response to neoadjuvant chemotherapy based on breast dce-mri. *Breast Cancer Research*, 19:1–14, 2 2017.

[11] W. Chen, M. Giger, G. Newstead, and U. Bick. Automatic identification and classification of characteristic kinetic curves of breast lesions on dce-mri. *Medical Physics*, 33:2878–2887, 8 2006.

[12] J. H. Chow and P. Kokotovic. Time scale modeling of sparse dynamic networks. *IEEE Transaction on Automatic Control*, 30:714–722, 3 1985.

[13] M. Dalmis, G. Litjens, K. Holland, A. Setio, R. Mann, N. Karssemeijer, and A. Gubern-Merida. Using deep learning to segment breast and fibroglandular tissue in mri volumes. *Medical Physics*, 44:533–546, 2017.

[14] F. De Pasquale, P Barone, G Sebastiani, and J Stander. Bayesian analysis of dynamic magnetic resonance breast images. *Applied Statistics*, pages 475–493, 2004.

[15] F. de Pasquale, M. Corbetta, V. Betti, and S. Della Penna. Cortical cores in network dynamics. *Neuroimage*, 180:370–382, 1 2018.

[16] B. Ellis and W. Hong. Learning causal bayesian network structures from experimental data. *Journal of the American Statistical Association*, 103:778–779, 11 2008.

[17] M. R. Emmett, R. Kroes, J. Moskal, C. Conrad, W. Priebe, F. Laezza, A. Meyer-Baese, and C. Nilsson. Integrative biological analysis for neuropsychopharmacology. *Neuropsychopharmacology*, 39:5–23, 11 2014.

[18] G. Ertas, O. Gulcur, O. Osman, O. Ucan, M. Tunaci, and M. Dursun. Breast mr segmentation and lesion detection with cellular neural networks and 3d template matching. *Computers in Biology and Medicine*, 38:116–126, 8 2008.

[19] A. Fornito, A. Zalesky, C. Pantelis, and E. Bullmore. Schizophrenia, neuroimaging and connectomics. *Neuroimage*, 62:2296–2314, 1 2012.

[20] Y. Gal, A. Mehnert, A. Bradley, D. Kennedy, and S. Crozier. New spatio-temporal features for improved discrimination of benign and malignant lesions in dynamic contrast-enhanced-magnetic resonance imaging of the breast. *Journal of Computer Assisted Tomography*, 35:645–652, 8 2011.

[21] C. Giessing and C. Thiel. Pro-cognitive drug effects modulate functional brain network organization. *Frontiers in Behavioral Neuroscience*, 6:1–9, 1 2012.

[22] A. Gliozzi, S. Mazzetti, P. Delsanto, D. Regge, and M. Stasi. Phenomenological universalities: a novel tool for the analysis of dynamic contrast enhancement in magnetic resonance imaging. *Physics in Medicine and Biology*, 56:573–586, 4 2011.

[23] R. Goerke. *An Algorithmic Walk from Static to Dynamic Graph Clustering*. PhD thesis, PhD thesis Karlsruhe Institute of Technology, 2010.

[24] C. Gössl, D. P. Auer, and L Fahrmeir. Bayesian spatiotemporal inference in functional magnetic resonance imaging. *Biometrics*, 57(2):554–562, 2001.

[25] C. Gössl, L Fahrmeir, and D. P. Auer. Bayesian modeling of the hemodynamic response function in BOLD fMRI. *NeuroImage*, 14:140–8, 2001.

[26] S. Hoffman, M. Lobbes, I. Houben, K. Pinker-Domenig, G. Lemaitre, G. Wengert, B. Burgeth, U. Meyer-Baese, and A. Meyer-Baese. Computer-aided diagnosis of diagnostically challenging lesions in breast mri: A comparison between a radiomics and a feature-selective approach. *SPIE Symposium Computational Intelligence*, page UNSP 98710H, 7 2016.

[27] S. Hoffmann, B. Burgeth, M. Lobbes, and A. Meyer-Baese. Automatic evaluation of single and joint kinetic and morphologic features for non-masses. *SPIE Symposium Computational Intelligence*, 8401:8401–38, 7 2012.

[28] S. Hoffmann, B. Burgeth, M. Lobbes, and A. Meyer-Baese. How effective is kinetic, morphologic, and mixed analysis for both mass and non-mass lesions? *SPIE Symposium Computational Intelligence*, 8401:8401–39, 7 2012.

[29] S. Hoffmann, J. D. Shutler, M. Lobbes, B. Burgeth, and A. Meyer-Baese. Automated analysis of diagnostically challenging lesions in breast mri based on spatio-temporal moments and joint segmentation-motion compensation technique. *EURASIP Journal on Advances in Signal Processing*, page 2013:172, 4 2013.

[30] B. Huynh, N. Antropova, and M. L. Giger. Comparison of breast dce-mri contrast time points for predicting response to neoadjuvant chemotherapy using deep convolutional neural network features with transfer learning. *SPIE Symposium Medical Imaging*, 10134:101340U, 2017.

[31] I. A. Illan, J. M. Gorriz, J. Ramirez, and A. Meyer-Baese. Spatial component analysis of mri data for alzheimer's disease diagnosis: a bayesian network approach. *Frontiers in Computational Neuroscience*, 8:1–9, 1 2014.

[32] F. Jamitzky, R. Stark, W. Bunk, S. Thalhammer, C. Räeth, T. Aschenbrenner, G. Morfill, and W. Heckl. Scaling-index method as an image processing tool in scanning-probe microscopy. *Ultramicroscopy*, 86:241–246, 2 2001.

[33] S. A. Jansen, A. Shimauchi, L. Zak, X. Fan, G. S. Karczmar, and G. M. Newstaed. The diverse pathology and kinetics of mass, nonmass, and focus enhancement on mr imaging of the breast. *Journal of Magnetic Resonance Imaging*, 33:1382–1389, 8 2011.

[34] L. Khedher, I. A. Illan, J. Gorriz, J. Ramirez, B. Abdelbasset, and A. Meyer-Baese. Independent component analysis-support vector machine-based computer-aided diagnosis system for alzheimer's with visual support. *International Journal of Neural Systems*, page DOI: 10.1142/S0129065716500507, 1 2016.

[35] S. Lall, J. Marsden, and S. Glavaski. A subspace approach to balanced truncation for model reduction of nonlinear control systems. *Int. Journal of Robust and Nonlinear Control*, February 2002.

[36] A. Lauric, E. Miller, M. Baharoglu, and A. Malek. 3d shape analysis of intracranial aneurysms using the writhe number as a discriminant for rupture. *Annals of Biomedical Engineering*, 39:1457–1469, 8 2011.

[37] A. Lauric, E. Miller, S. Frisken, and A. Malek. Automated detection of intracranial aneurysms based on parent vessel 3d analysis. *Medical Image Analysis*, 14:149–159, 8 2010.

[38] Y. LeCun, Y. Bengio, and G. Hinton. Deep learning. *Nature*, 521:436–444, 1 2015.

[39] S. Lee, J. Kim, Z. Yang, Y. Jung, and W. Moon. Multilevel analysis of spatiotemporal association features for differentiation of tumor enhancement pattern in breast dce-mri. *Medical Physics*, 37:3940–3956, 7 2010.

[40] J. Li, M. Fan, J. Zhang, and L. Li. Discriminating between benign and malignant breast tumors using 3d convolutional neural network in dynamic contrast enhanced-mr images. *SPIE Medical Imaging*, 10138:UNSP1013808, 2017.

[41] D. Liu, C. Yan, J. Ren, L. Yao, V. Kiviniemi, and Y. Zang. Using coherence to measure regional homogeneity of resting-state fmri signal. *Frontiers in Systems Neuroscience*, 6:1–9, 1 2012.

[42] Y. Liu, J. Slotine, and A. Barabasi. Controllability of complex networks. *Nature*, 473:167–173, 12 2011.

[43] Z. Liu, Z. Li, J. Qu, R. Zhang, X. Zhou, L. Li, K. Sun, Z. Tang, H. Jiang, H. Li, Q. Xiong, Y. Ding, X. Zhao, K. Wang, Z. Liu, and J. Tan. Radiomics of multiparametric mri for pretreatment prediction of pathologic complete response to neoadjuvant chemotherapy in breast cancer: A multicenter study. *Clinical Cancer Research*, 25:3538–3547, 2019.

[44] S. Mazzetti, A. Gliozzi, C. Bracco, F. Russo, D. Regge, and M. Stasi. Comparison between pun and tofts models in the quantification of dynamic contrast-enhanced mr imaging. *Physics in Medicine and Biology*, 57:8443–8453, 4 2012.

[45] L. Arbash Meinel, A. Stolpen, K. Berbaum, L. Fajardo, and J. Reinhardt. Breast mri lesion classification: Improved performance of human readers with a backpropagation network computer-aided diagnosis (cad) system. *Journal of Magnetic Resonance Imaging*, 25:89–95, 8 2007.

[46] M. Mesbahi and M. Egerstedt. *Graph Theoretic Methods in Multiagent Networks*. Princeton University Press, 2010.

[47] A. Meyer-Baese, , O. Lange, T. Schlossbauer, and A. Wismueller. Computer-aided diagnosis and visualization based on clustering and independent component analysis for breast mri. *ICIP2008*, 3:3000–3003, 1 2008.

[48] A. Meyer-Baese, A. Moradi Amani, U. Meyer-Baese, S. Foo, A. Stadlbauer, and W. Yu. Pinning observability of competitive neural networks with different time constants. *Neurocomputing*, In press, 1 2018.

[49] A. Meyer-Baese, R. Goerke, D. Wagner, H. He, M. Emmett, A. Marshall, and C. Conrad. Determining and interpreting correlations in lipidomic networks found in glioblastoma cells. *BMC Systems Biology*, 4:126–136, 7 2010.

[50] A. Meyer-Baese, R. Goerke, D. Wagner, H. He, M. Emmett, A. Marshall, and C. Conrad. Determining and interpreting correlations in lipidomic networks found in glioblastoma cells. *SPIE Symposium Computational Intelligence*, 7704:770406, 7 2010.

[51] A. Meyer-Baese, A. Koshkouei, M. Emmett, and D. Goodall. Global stability analysis and robust design of multi-time-scale biological networks under parametric uncertainties. *Neural Networks*, 22:658–663, 7 2009.

[52] A. Meyer-Baese, R. Roberts, I. Illan, U. Meyer-Baese, M. Lobbes, A. Stadlbauer, and K. Pinker-Domenig. Dynamical graph theory networks methods for the analysis of sparse functional connectivity networks and for determining pinning observability in brain networks. *Frontiers in Computational Neuroscience*, https://doi.org/10.3389/fncom.2017.00087, 1 2017.

[53] A. Meyer-Baese, R. Roberts, and V. Thuemmler. Local uniform stability of competitive neural networks with different time-scales under vanishing perturbations. *Neurocomputing*, 73:770–775, 4 2010.

[54] A. Meyer-Baese, R. Roberts, and H. Yu. Robust stability analysis of competitive neural networks with different time-scales under perturbations. *Neurocomputing*, 71:417–420, 11 2007.

[55] A. Meyer-Baese and F. Theis. Gene regulatory networks simplified by nonlinear balanced truncation. *SPIE Symposium Computational Intelligence*, 6979:6979C, 7 2008.

[56] A. Meyer-Baese and V. Thummler. Local and global stability analysis of an unsupervised competitive neural network. *IEEE Transactions on Neural Networks*, 19:346–351, 5 2008.

[57] U. Meyer-Baese, A. Vera, A. Meyer-Baese, M. Pattichis, and R. Perry. Discrete wavelet-transform fpga using matlab/simulink. *SPIE's 20th Annual International Symposium on Aerospace/ Defense Sensing, Simulation and Controls, Vol. 6247*, page 624703, 9 2006.

[58] A. Meyer-Bäse. Gene regulatory networks simplified by nonlinear balanced truncation. *SPIE Proceedings Series*, 6979:69790C, 4 2008.

[59] A. Meyer-Bäse, R. Watzeland U. Meyer-Bäse, and S. Foo. A parallel CORDIC architecture dedicated to compute the gaussian potential function in neural networks. *Engineering Applications of Artificial Intelligence*, 16:595–605, October-December 2003.

[60] A. Meyer-B"ase, U. Meyer-B"ase, J. Mellott, and F. Taylor. A fast modified cordic–implementation of radial basis neural networks. *Journal of VLSI SIGNAL PROCESSING SYSTEMS for Signal, Image, and Video Technology*, pages 290–298, 9 1998.

[61] A. Meyer-Bäse, F. Theis, and C. Conrad. Uncertain gene regulatory networks simplified by gramian-based approach. *International Conference on Bioinformatics and Computational Biology 2011*, page In print, 4 2011.

[62] A. Meyer-B"ase, R. Watzel, U. Meyer-B"ase, and S. Foo. A parallel cordic architecture to compute the gaussian potential function in neural networks. *Engineering Application of Artificial Intelligence*, pages 595–605, 9 2003.

[63] U. Meyer-Bäse, A. Meyer-Bäse, J. Mellott, and F. Taylor. A fast modified CORDIC-implementation of radial basis neural networks. *Journal of VLSI SIGNAL PROCESSING SYSTEMS for Signal, Image and Video Technology*, 9:290–298, 1998.

[64] B. Moore. Principal component analysis in linear systems: controllability, observability and model reduction. *IEEE Transactions on Automatic Control*, pages 17–32, January 1981.

[65] D. Newell, K. Nie, J. Chen, C. Hsu, H. Yu, O. Nalcioglu, and M. Su. Selection of diagnostic features on breast mri to differenetiate between malignant and benign lesions using computer-aided diagnostics: Differences in lesions presenting as mass and non-mass-like enhancement. *European Radiology*, 20:771–781, 2 2010.

[66] D. Ngo, M. Lobbes, M. Lockwood, and A. Meyer-Baese. Spatio-temporal feature extraction for differentiation of non-mass-enhancing lesions in breast mri. *SPIE Symposium Computational Intelligence*, 8367:8367–9, 7 2012.

[67] P. Prasann, P. Tiwari, and A. Madabhushi. Co-occurence of local anisotropic gradient orientations (collage): A new radiomics descriptor. *Scientific Reports*, 6:37241, 7 2016.

[68] K. Ravichandran, N. Braman, A. Janowczyk, and A. Madabhushi. A deep learning classifier for prediction of pathological complete response to neoadjuvant chemotherapy from baseline breast dce-mri. *SPIE Medical Imaging*, 10575:UNSP10575C, 2018.

[69] F. Retter, C. Plant, B. Burgeth, G. Botilla, T. Schlossbauer, and A. Meyer-Baese. Computer-aided diagnosis for diagnostically challenging breast lesions in dce-mri based on image registration and integration of morphologic and dynamic characteristics. *EURASIP Journal on Advances in Signal Processing*, page 2013:157, 4 2013.

[70] Ali Saberi and Hassan Khalil. Quadratic–type lyapunov functions for singularly perturbed systems. *IEEE Transactions on Automatic Control*, pages 542–550, June 1984.

[71] A. Saha, X. Z. Yu, D. Sahoo, and M. Mazurowski. Effects of mri scanner parameters on breast cancer radiomics. *Expert Systems with Applications*, 87:384–391, 2017.

[72] B. Sahiner, H. P. Chan, N. Petrick, D. Wei, M. A. Helvie, D. Adler, and M. M. Goodsitt. Classification of mass and normal breast tissue: A convolution neural network classifier with spatial domain and texture images. *IEEE Transaction on Medical Imaging*, 15:598–610, 10 1996.

[73] J. Scherpen. Balancing for nonlinear systems. *Systems and Control Letters*, pages 143–153, March 1993.

[74] Volker J. Schmid, Brandon Whitcher, Anwar R. Padhani, N Jane Taylor, and Guang-Zhong Yang. Bayesian methods for pharmacokinetic models in dynamic contrast-enhanced magnetic resonance imaging. *IEEE Transactions on Medical Imaging*, 25(12):1627–36, 2006.

[75] J. Shi, B. Sahiner, H. Chan, C. Paramagul, L. Hadjinski, M. Helvie, and T. Chenevert. Treatment response assessment of breast masses on dynamic contrast-enhanced magnetic resonance scans using fuzzy c-means clustering and level set segmentation. *Medical Physics*, 36:5052–5063, 8 2009.

[76] J. D. Shutler and M. S. Nixon. Zernike velocity moments for sequence-based description of moving features. *Image Vision Comput.*, 24:343–356, 4 2006.

[77] A. Smith, A. Ehtemami, D. Fratte, A. Meyer-Baese, O. Zavala-Romero, A. Goudriaan, L. Schmaal, and M. Schulte. Functional connectivity analysis of resting-state fmri networks in nicotine dependent patients. *Medical Imaging 2016: Biomedical Applications in Molecular, Structural, and Functional Imaging*, 9788:978827, 1 2016.

[78] M. Stoutjesdijk, J. Veltman, H. Huisman, N. Karssemeijer, J. Barentsz, J. Blickman, and C. Boetes. Automated analysis of contrast enhancement in breast mri lesions using mean shift clustering for roi selection. *Journal Magnetic Resonance Imaging*, 26:606–614, 2 2007.

[79] B. Szabo, M. Wilberg, B. Bone, and P. Aspelin. Application of artificial neural networks to the analysis of dynamic mr imaging features to the breast. *European Radiology*, 14:1217–1225, 2 2004.

[80] A. Tahmassebi, G. Wengert, T. Helbich, Z. Bago-Horvath, S. Alaei, R. Bartsch, P. Dubsky, P. Baltzer, P. Clauser, P. Kapetas, E. Morris, A. Meyer-Baese, and K. Pinker. Impact of machine learning with multiparametric magnetic resonance imaging of the breast for early prediction of response to neoadjuvant chemotherapy and survival outcomes in breast cancer patients. *Investigative Radiology*, DOI: 10.1097/RLI.0000000000000518, 1 2018.

[81] J. Tanabe, E. Nyberg, L. Martin, D. Cordes, E. Kronberg, and J. Tregallas. Nicotine effects on default mode network during resting state. *Psychopharmacology*, 216:287–295, 4 2011.

[82] Y. Tang, Z. Wang, H. Gao, S. Swift, and J. Kurths. A constrained evolutionary compuattion method for detecting controlling regions of cortical networks. *IEEE/ACM Transactions on computational biology and bioinformatics*, 9:1569–1581, 1 2012.

[83] F. Theis and A. Meyer-Bäse. *Biomedical Signal Analysis: Contemporary Methods and Applications*. MIT Press, 2010.

[84] D. Wheland, A. Joshi, K. McMahon, N. Hansell, N. Martin, M. Wright, P. Thomson, D. Shattuk, and R. Leahy. Robust identification of partial-correlation based networks with applications to cortical thickness data. *9th IEEE International Symposium on Biomedical Imaging (ISBI)*, 3:1551–1554, 5 2012.

[85] K. Wylie, D. Rojas, J. Tanabe, L. Martin, and J. Tregallas. Nicotine increases brain functional network efficiency. *Neuroimage*, 63:73–80, 1 2012.

[86] P. Yap, R. Paramesran, and S. Ong. Image analysis by krawtchouk moments. *IEEE Transactions on Image Processing*, 12:1367–1377, 9 2003.

[87] R. Yu, L. Zhao, W. Qin, W. Wang, K. Yuan, Q. Li, and L. Lu. Regional homogeneity changes in heavy male smokers: a resting-state functional magnetic resonance imaging study. *Addiction Biology*, pages j.1369–1600, 4 2011.

[88] W. Yu, G. Chen, and M. Cao. Consensus in directed newtorks of agents with nonlinear dynamics. *IEEE Transactions on Automatic Control*, 56:1436–1441, 5 2011.

[89] L. Zeng, H. Shen, L. Liu, L. Wang, B. Li, P. Fang, Z. Zhou, Y. Li, and D. Hu. Identifying major depression using whole-brain functional connectivity: a multivariate pattern analysis. *Brain*, 1498:1498–1507, 4 2012.

[90] J. Zhang, A. Saha, Z. Zhu, and M. Mazurowski. Breast tumor segmentation in dce-mri using fully convolutional networks with an application in radiogenomics. *SPIE Medical Imaging*, 10575:UNSP10575oU, 2018.

[91] J. Zhu, E. Alwadawy, A. Saha, Z. Zhang, H. Harowicz, and M. Mazurowski. Breast cancer molecular subtype classification using deep features: Preliminary results. *SPIE Medical Imaging*, 10575:UNSP105752X, 2018.